Agricultural and Forest Meteorology 222 (2016) 87–97

Contents lists available at ScienceDirect

Agricultural and Forest Meteorology

journal homepage: www.elsevier.com/locate/agrformet

Parameterizing ecosystem light use efficiency and water use efficiency to estimate maize gross primary production and evapotranspiration using MODIS EVI

Pradeep Wagle[a,*,1], Prasanna H. Gowda[b], Xiangming Xiao[a,c], Anup KC[d]

[a] Department of Microbiology and Plant Biology, and Center for Spatial Analysis, University of Oklahoma, Norman, OK 73019, USA
[b] USDA-ARS Grazinglands Research Laboratory, El Reno, OK 73036, USA
[c] Institute of Biodiversity Science, Fudan University, Shanghai, China
[d] Department of Natural Resource Ecology and Management, Oklahoma State University, Stillwater, OK 74078, USA

ARTICLE INFO

Article history:
Received 23 October 2015
Received in revised form 17 March 2016
Accepted 18 March 2016

Keywords:
Artificial neural network
Eddy covariance
Empirical and statistical models
Remote sensing
Seasonal and interannual variability
Vegetation indices

ABSTRACT

Quantifying global carbon and water balances requires accurate estimation of gross primary production (GPP) and evapotranspiration (ET), respectively, across space and time. Models that are based on the theory of light use efficiency (LUE) and water use efficiency (WUE) have emerged as efficient methods for predicting GPP and ET, respectively. Currently, LUE and WUE estimates are obtained from biome-specific look-up tables and coarse resolution remote sensing data with large uncertainties. The major objective of this study was to parameterize eddy covariance tower-based ecosystem LUE ($ELUE_{EC}$), defined as the ratio of tower-based GPP (GPP_{EC}) to photosynthetically active radiation (PAR), and ecosystem WUE ($EWUE_{EC}$), defined as the ratio of GPP_{EC} to tower-based ET (ET_{EC}), using the Moderate Resolution Imaging Spectroradiometer (MODIS)-derived enhanced vegetation index (EVI) for predicting maize (*Zea mays* L.) GPP and ET, respectively. Three adjacent AmeriFlux maize sites with different rotations (continuous maize vs. annual rotation of maize and soybean, *Glycine max* L.) and water management practices (rainfed vs. irrigated) located near Mead, NE, USA were selected. The EVI tracked the seasonal variations of $ELUE_{EC}$ ($R^2 = 0.83$) and $EWUE_{EC}$ ($R^2 = 0.74$) across sites, indicating that EVI can be explicitly used as a measure of $ELUE_{EC}$ and $EWUE_{EC}$. The predicted GPP (GPP_{ELUE}) using the parameterized ELUE model correlated well with GPP_{EC} (slope = 1.0, $R^2 = 0.83$, and RMSE = 2.85 g C m^{-2} d^{-1}) and was significantly improved when compared to widely used models that estimate GPP by integrating EVI and climate variables (Greenness and Radiation, Temperature and Greenness, and Vegetation Index) and the standard MOD17 GPP product. Similarly, the predicted ET (ET_{EWUE}) using the parameterized EWUE correlated well with ET_{EC} (slope = 1.02, $R^2 = 0.62$, and RMSE = 0.83 mm ET^{-1}) and was significantly improved when compared to the standard MOD16 ET product. Preliminary data demonstrate that ELUE and EWUE can be parameterized using EVI, offering new methods for predicting GPP and ET.

© 2016 Elsevier B.V. All rights reserved.

1. Introduction

Accurate estimation of gross primary production (GPP) and evapotranspiration (ET) across space and time is crucial to quantify global carbon and water balances, respectively. Eddy covariance (EC) systems can measure carbon uptake and water losses by ecosystems at the landscape level (Baldocchi et al., 2001). However, these EC measurements are representative of fluxes only from within the EC tower footprint. Satellite remote sensing approach can complement the limited coverage of GPP and ET estimates by EC systems. Consequently, a variety of methods that leverage remotely-sensed products to predict GPP and ET have been developed and validated using EC data.

Current remote sensing estimations of GPP fall into two broad approaches. The first approach is to estimate GPP based on the theory of light use efficiency (LUE) proposed by Monteith (1972). Several existing broad-scale carbon flux models such as Moderate Resolution Imaging Spectroradiometer Photosynthesis, MODIS-PSN (Running et al., 2004), Carnegie–Ames–Stanford Approach, CASA (Potter et al., 1993), Global Production Efficiency Model, GLO-

* Corresponding author.
E-mail addresses: pradeep.wagle@ou.edu, pradeep.wagle@okstate.edu (P. Wagle).
[1] Office address: USDA-ARS Grazinglands Research Laboratory, El, Reno, OK, 73036, USA.

http://dx.doi.org/10.1016/j.agrformet.2016.03.009
0168-1923/© 2016 Elsevier B.V. All rights reserved.

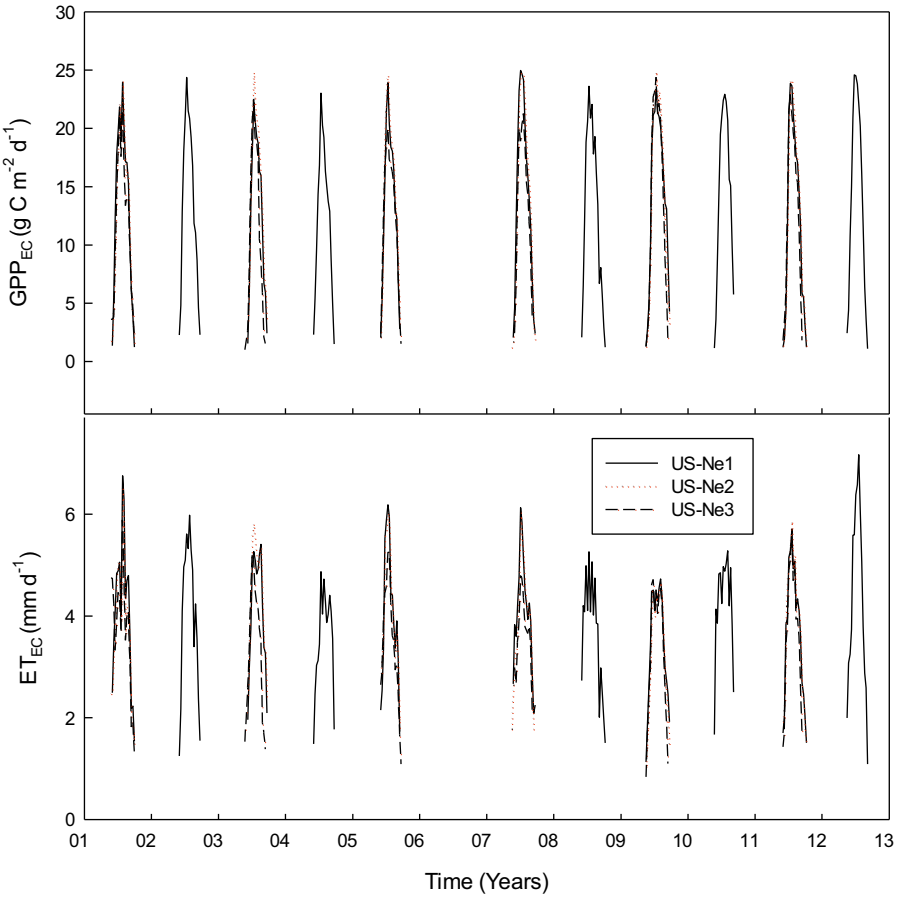

Fig. 1. Seasonality and interannual dynamics of tower-based gross primary production (GPP_{EC}) and evapotranspiration (ET_{EC}) at three maize sites.

PEM (Prince and Goward, 1995), Vegetation Photosynthesis Model, VPM (Xiao et al., 2004), and Eddy Covariance Light Use Efficiency Model, EC-LUE (Yuan et al., 2007) follow the fundamental GPP estimation method (Monteith, 1972) as:

$$GPP = \varepsilon \times fAPAR \times PAR \quad (1)$$

where ε is light use efficiency, PAR is photosynthetically active radiation, and fAPAR is the fraction of PAR absorbed by vegetation. In Eq. (1), separate estimations of fAPAR and ε are required to compute GPP for the current LUE-based models. A major limitation for this GPP estimation approach is that direct measurements of LUE are not available at the landscape scale. Conclusive results have not been achieved to directly compute LUE even by using narrow-band vegetation indices such as photochemical reflectance index, PRI (Gamon et al., 1992) and solar-induced chlorophyll fluorescence, SIF (Parazoo et al., 2014). Even though the PRI performance is good at leaf or plant levels, it is problematic at the ecosystem level when using MODIS data (Moreno et al., 2012; Tan et al., 2013). Further, parameterization of LUE is difficult as it is influenced by vegetation types (Turner et al., 2003), seasonality and plant phenology (Jenkins et al., 2007), and environmental stresses (Ruimy et al., 1995). Due to these reasons, maximum LUE values have been specified for a limited number of biome types and are available in vegetation-specific look-up table. In most LUE-based models, a constant potential or maximum LUE value is used and then down-regulated by environmental constraints (Running et al., 2004).

Differences in the GPP estimates from LUE-based models are generally due to differences in the determination or selection of LUE and the use of environmental stress scalars. The second remote sensing GPP estimation approach is the development of empirical/statistical models based on tower-based GPP (GPP_{EC}), climate variables, and remotely-sensed vegetation indices (Gitelson et al., 2006; Sims et al., 2008; Wu et al., 2010) and most recently based on GPP_{EC} and SIF (Guanter et al., 2014; Wagle et al., 2015c).

Remote sensing estimations of ET also fall broadly into two approaches. The first approach is to estimate ET using physical models based on the surface energy balance (SEB) concept (Gillies et al., 1997). Several SEB models have been developed in past two decades to estimate large-scale ET (Allen et al., 2007; Bastiaanssen et al., 1998; Roerink et al., 2000; Senay et al., 2013; Su, 2002). Those SEB models typically estimate sensible heat flux (H) from the difference between ground-based air temperature (T_a) and satellite-based land surface temperature (LST). The lack of 1:1 correspondence between LST and aerodynamic surface temperature poses a number of difficulties in estimating H (Kustas and Norman, 1996) and ultimately reliable ET estimates. Further, relatively complex computation of several land surface physical parameters and turbulent heat fluxes, and too many required parameters with detailed information in physically-based models can cause more inconveniences and uncertainties when data are not readily available (Liou and Kar, 2014). Several surface variables like land surface temperature, surface albedo, soil moisture, emissivity, fractional vegetation cover, leaf area index can significantly affect the precise partition of energy components and consequently the accuracy of SEB models. The second remote sensing ET estimation approach is the development of empirical/statistical models (Choudhury et al., 1994) based on tower-based ET (ET_{EC}), vegetation indices, and climate variables. Increasing number of flux towers and availability of remote sensing vegetation indices offer a tool for upscaling of ecosystem level measurements of ET over large areas (Glenn et al.,

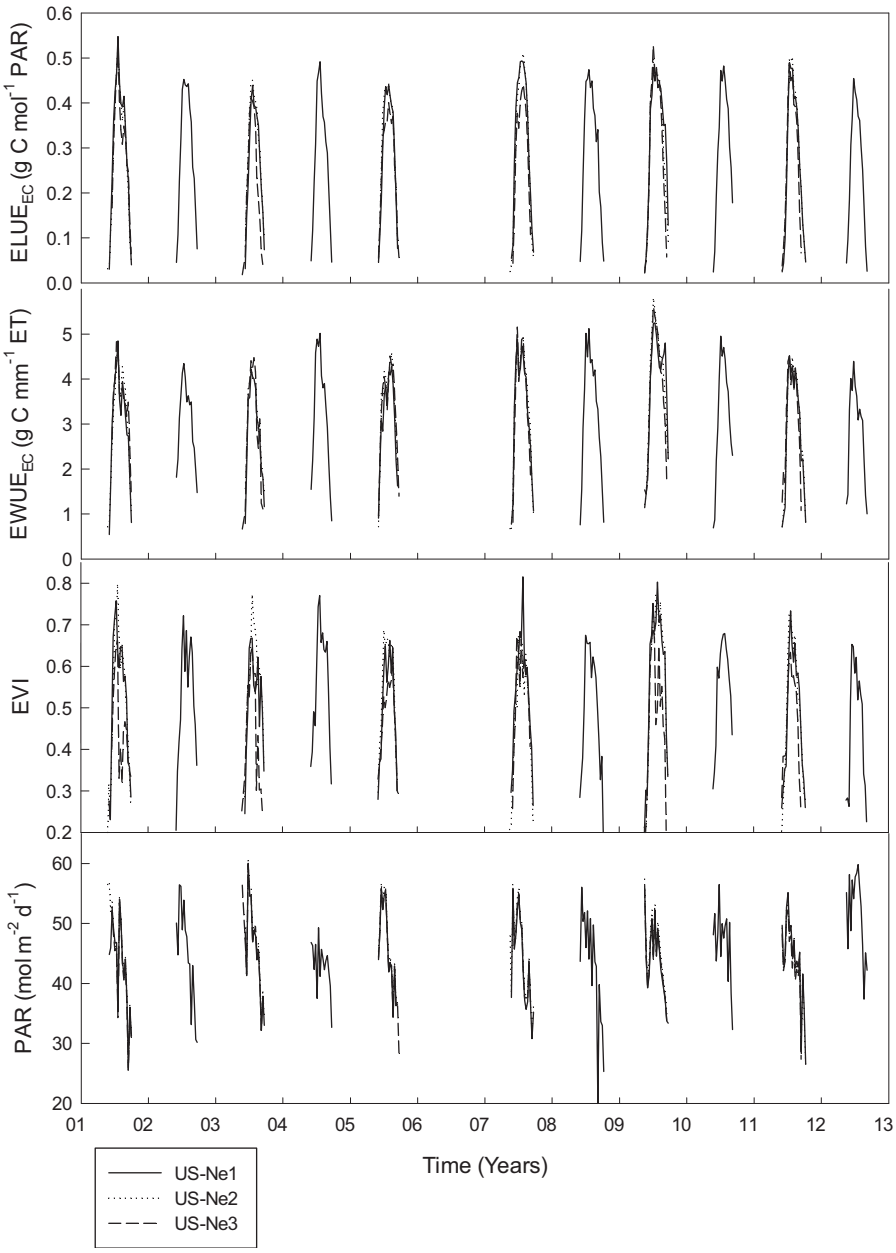

Fig. 2. Seasonality and interannual dynamics of tower-based ecosystem light use efficiency ($ELUE_{EC}$), ecosystem water use efficiency ($EWUE_E$), enhanced vegetation index (EVI), and photosynthetically active radiation (PAR) at three maize sites.

2007). The empirical approach directly uses vegetation indices in scaling ET rather than using them to compute several canopy properties to be used as parameters in physically-based models (Bonan, 1993; Glenn et al., 2007). It is also important to note that flux towers do not require knowledge of leaf area index, fraction cover, and details of canopy architecture to provide results, and they provide measurements of fluxes at scales that can partly or fully overlap the pixel size of satellite sensors (Glenn et al., 2007). Thus, the empirical approach can constrain satellite data and minimize the uncertainty involved in ET estimates. Consequently, integration of vegetation indices with flux tower data is more robust and suitable scaling tool rather than solving complex equations of physical models with limited input data (Glenn et al., 2008). Furthermore, vegetation indices are more robust because they are computed the same way regardless of surface conditions across all pixels in time and space. The comparison of ET estimation methods showed that more complex physical and analytical methods were not necessarily more accurate than simple statistical and empirical methods (Kalma et al., 2008). The empirical approach, therefore, can be used as a simple and alternative approach to provide reasonably accurate estimates of ET when ground-based data are available and/or input data are limited to solve complex physically-based models.

Similar to maximum values of ecosystem light use efficiency (ELUE), maximum values of ecosystem water use efficiency (EWUE) are also considered as a relatively constant for a biome type and similar across many of the world's major biomes (Law et al., 2002). It is important to note that EWUE is different from just the water use efficiency (WUE) of individual plant species as EWUE is influenced by several other factors such as heterotrophic respiration, decomposition of organic materials, and evaporation of moisture from the soil surface (Emmerich, 2007). Consequently, large spatial and temporal variability in EWUE was reported for the same plant functional type (i.e., grasslands) across the United States (Wagle et al., 2015a), illustrating that EWUE is not a constant property for

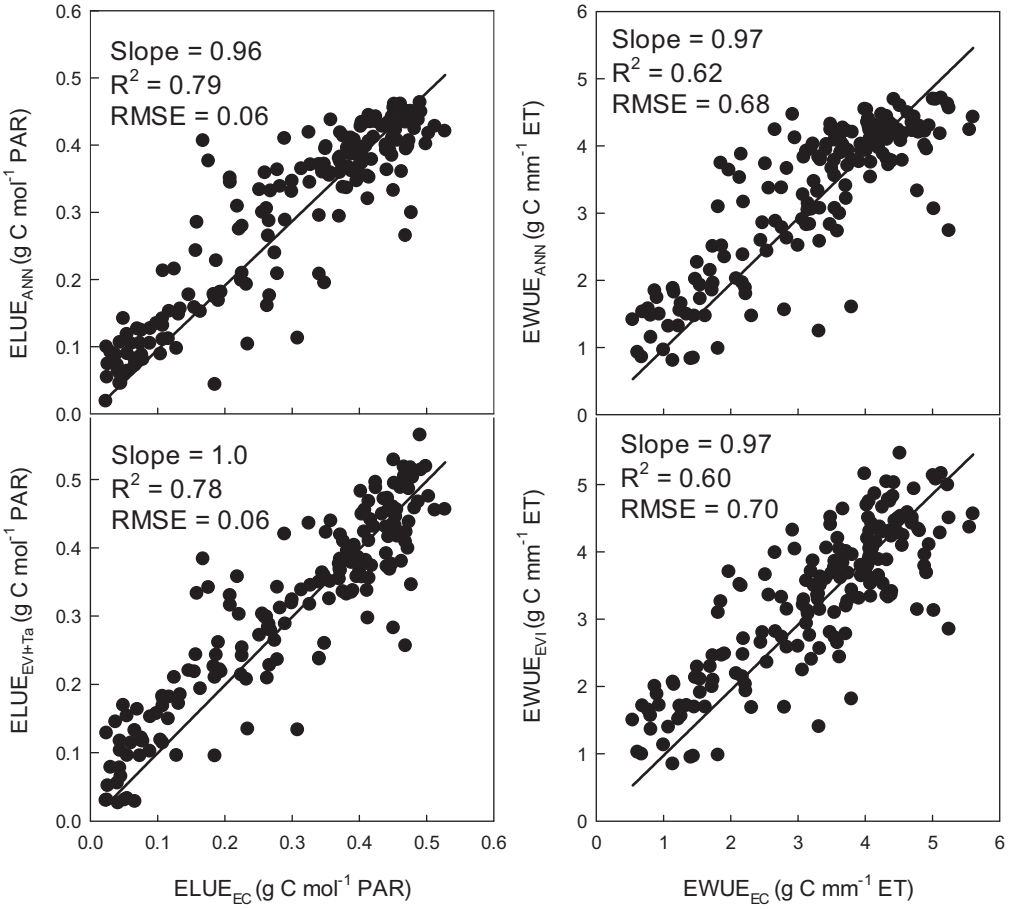

Fig. 3. Linear comparisons of predicted ecosystem light use efficiency ($ELUE_{EVI+Ta}$ and $ELUE_{ANN}$) and ecosystem water use efficiency ($EWUE_{EVI+Ta}$ and $EWUE_{ANN}$) using regression and artificial neural network (ANN) models with tower-based $ELUE_{EC}$ and $EWUE_{EC}$ for the model validation dataset. R^2: the coefficient of determination and RMSE: root mean square error.

a biome type. Thus, improved representation of spatial and temporal differences in ELUE and EWUE is crucial for better modeling results.

Previous studies have reported strong correlations between GPP/PAR (=ELUE) and canopy total chlorophyll content (Wu et al., 2009) or enhanced vegetation index, EVI (Ma et al., 2014), and between GPP/ET (=EWUE) and EVI (Tang et al., 2015; Zhang et al., 2009). Ma et al. (2014) parameterized ELUE using EVI and PAR to estimate savanna GPP. A new algorithm that uses EVI and LST was proposed to estimate monthly forest LUE (Wu et al., 2012). Based on those results, we hypothesized that a robust relationship could be established by integrating EVI and climate variables with ELUE and EWUE to accurately estimate maize (*Z. mays* L.) GPP and ET, respectively. This approach not only provides direct estimations of ELUE and EWUE but also offers new methods for predicting GPP and ET. Further, this method simplifies remote sensing-based GPP and ET estimates, and also reduces uncertainties involved with the use of biome-specific maximum ELUE and EWUE values in GPP and ET models.

The objectives of this study were (1) to understand seasonal dynamics and interannual variations in ELUE and EWUE derived from EC measurements, and (2) to parameterize ELUE and EWUE using EVI to estimate maize GPP and ET, respectively. Further, this study compares the performance of the parameterized ELUE model to several commonly used GPP models: Greenness and Radiation, GR (Gitelson et al., 2006), Temperature and Greenness, TG (Sims et al., 2008), and Vegetation Index, VI (Wu et al., 2010), the standard global MOD17 GPP product, GPP_{MOD17} (Running et al., 2004), and statistical models developed in this study using GPP_{EC} data. Similarly, the performance of the parameterized EWUE model is compared with the standard MOD16 ET product, ET_{MOD16} (Mu et al., 2007), and statistical models developed in this study using ET_{EC} data.

Table 1
Pearson correlation coefficients (r) between tower-based gross primary production (GPP_{EC}), evapotranspiration (ET_{EC}), ecosystem light use efficiency ($ELUE_{EC}$), and ecosystem water use efficiency ($EWUE_{EC}$) versus enhanced vegetation index (EVI), air temperature (T_a), and photosynthetically active radiation (PAR) for the entire dataset (8-day values) at three maize sites. The highest r value for each response variable is highlighted in bold.

Variable	GPP_{EC}	ET_{EC}	$ELUE_{EC}$	$EWUE_{EC}$
T_a	0.64	0.71	0.58	0.48
EVI	0.87	0.74	0.91	**0.86**
PAR	0.48	0.57	0.27	0.27
EVI × T_a	0.91	0.83	**0.92**	0.83
EVI × PAR	**0.93**	**0.86**	0.86	0.82

2. Materials and methods

2.1. Site description

Three adjacent study sites (US-Ne1, US-Ne2, and US-Ne3) are located at the University of Nebraska Agricultural Research and Development Center, near Mead, NE. These sites have similar climatic conditions as they are located within 1.6 km of each other. The US-Ne1 site is irrigated continuous maize using a center pivot

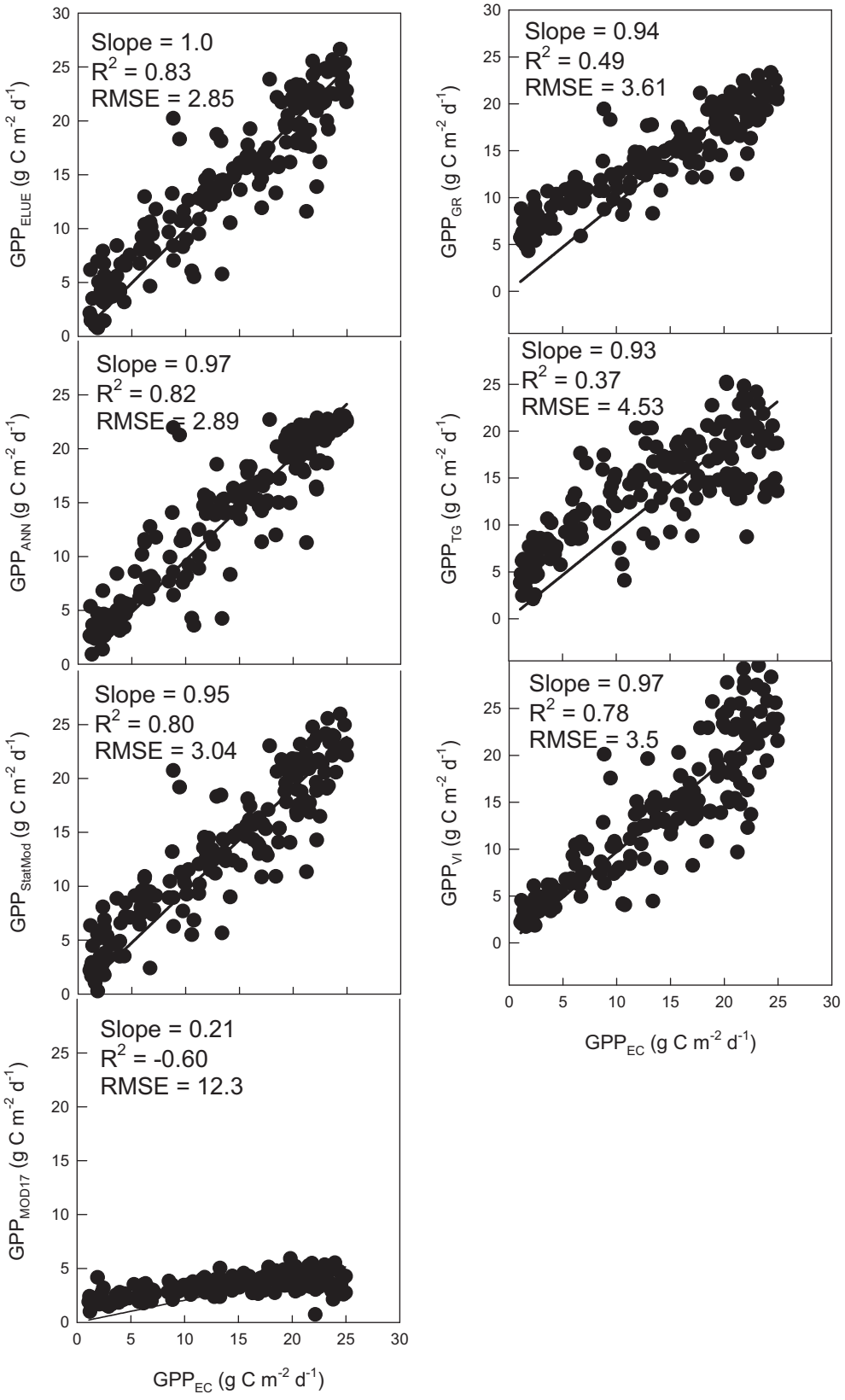

Fig. 4. Linear comparisons of tower-based gross primary production (GPP_{EC}) with GPP estimates from several models for the model validation dataset.R^2: the coefficient of determination and RMSE: root mean square error ($g\,C\,m^{-2}\,d^{-1}$).

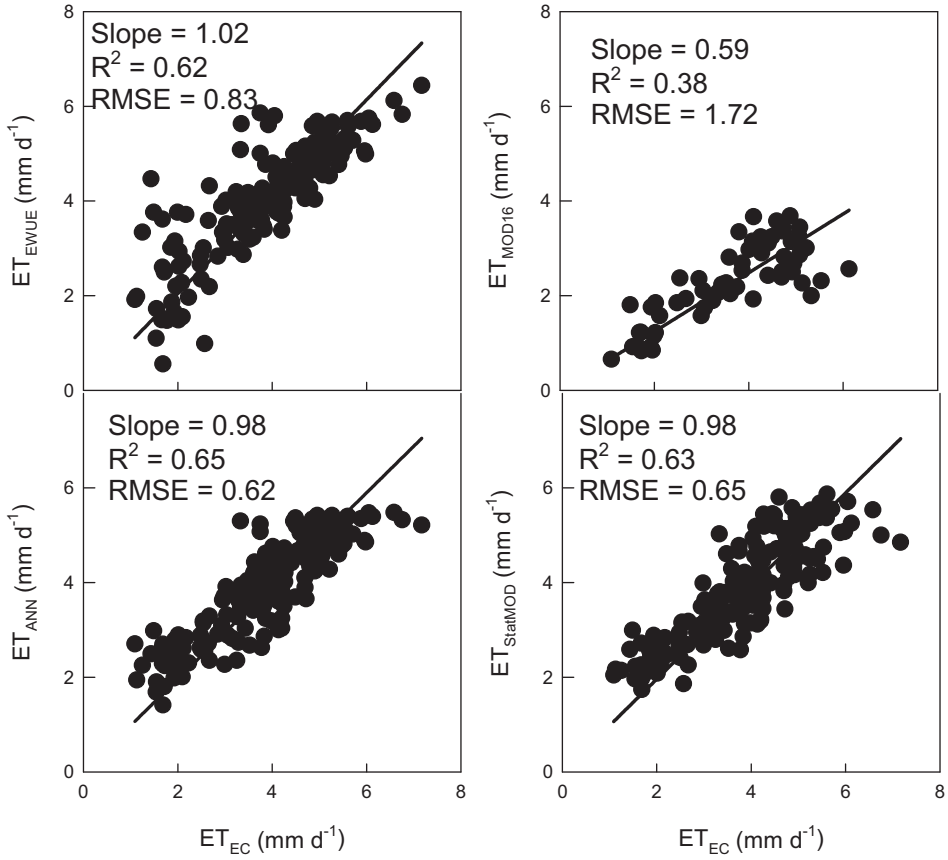

Fig. 5. Linear comparisons of tower-based evapotranspiration (ET_{EC}) with ET estimates from several models for the model validation dataset. R^2: the coefficient of determination and RMSE: root mean square error (mm d^{-1}).

irrigation system. The US-Ne2 and US-Ne3 are maize and soybean (*Glycine max* L.) rotation sites, with maize planted in odd years. The difference between US-Ne2 and US-Ne3 sites is the US-Ne2 site is irrigated using a center pivot irrigation system and the US-Ne3 is rainfed. Detailed site information is available in previous studies (Suyker and Verma, 2012; Verma et al., 2005) or on the AmeriFlux website (http://ameriflux.lbl.gov/).

2.2. Eddy flux and ground-based climate data

Carbon and water vapor fluxes at all three sites were measured using the EC technique. The gap-filled flux data (GPP_{EC} and ET_{EC}) and site-specific climate data (PAR and T_a) were obtained from the AmeriFlux website (http://ameriflux.lbl.gov/). We used 11 years of data (2001–2012, missing 2006) from US-Ne1 and six years of data from both US-Ne2 and US-Ne3 (2001–2011, odd years with maize crop only) sites. The flux and climate data were composited for 8-day intervals to match the temporal resolution of the MODIS-derived EVI.

2.3. MODIS products

2.3.1. MODIS EVI and LST products

We obtained 8-day composite 500 m surface reflectance product (MOD09A1) to compute EVI and 8-day 1-km MODIS global daytime LST product (MOD11A2) to compute LST for each flux tower site (one MODIS pixel surrounding the flux tower site) from the MODIS data portal at the Earth Observation and Modeling Facility (EOMF), University of Oklahoma (http://eomf.ou.edu/visualization/). The observations with the bad quality flags (i.e., clouds or cloud shadows) in both MOD09A1 and MOD11A2 products were gap-filled using a linear interpolation method (Jin et al., 2013).

2.3.2. MODIS GPP and ET products

The global GPP_{MOD17} and ET_{MOD16} products are available at 1-km spatial resolution. We obtained 8-day composite values of GPP_{MOD17} and ET_{MOD16} for the MODIS pixels surrounding each flux site from the Oak Ridge National Laboratory Distributed Active Archive Center (ORNL DAAC) website (http://daac.ornl.gov/MODIS/modis.shtml). The GPP_{MOD17} and ET_{MOD16} datasets were used only to compare with our models.

2.4. Parameterization of $ELUE_{EC}$ and $EWUE_{EC}$

We computed $ELUE_{EC}$ (g C mol^{-1} PAR) and $EWUE_{EC}$ (g C mm^{-1} ET) as:

$$ELUE_{EC} = \frac{GPP_{EC}}{PAR} \quad (2)$$

$$EWUE_{EC} = \frac{GPP_{EC}}{ET_{EC}} \quad (3)$$

We developed time series of $ELUE_{EC}$ and $EWUE_{EC}$ at 8-day intervals to match the temporal resolution of the MODIS-derived EVI. The dataset from all three sites (n = 354 samples) were first randomized, then divided into two equal subsets (n = 177 each for model calibration and validation). For the calibration dataset, simple and multiple regression analyses of $ELUE_{EC}$ and $EWUE_{EC}$ against major controlling variables (EVI, PAR, and T_a) were performed to obtain the best predictive equation for ELUE ($ELUE_{Pred}$) and EWUE

Table 2
A comparison of performance of regression and artificial neural network models for predicting gross primary production (GPP), evapotranspiration (ET), ecosystem light use efficiency (ELUE), and ecosystem water use efficiency (EWUE). A simple and robust regression model for each response variable is highlighted in bold.

S.N.	Equation	Model	R^2	AIC	SBC
Response variable: GPP					
1	−8.55 + 42.98 EVI	LR	0.79	438.54	444.89
2	−5.06 + 1.58 T_a × EVI	LR	0.86	366.36	372.71
3	**−5.53 + 0.81 EVI × PAR**	**LR**	**0.88**	**339.35**	**345.70**
4	−19.22 + 36.40 EVI + 0.68 PAR	MR	0.85	379.01	388.53
5	−19.22 + 36.40 EVI + 0.62 T_a	MR	0.85	379.01	388.53
6	−21.45 + 36.79 EVI + 0.19 PAR + 0.33 T_a	MR	0.87	349.74	362.45
7	Artificial Neural Network		–	302.58	343.87
Response variable: ET					
1	0.61 + 6.29 EVI	LR	0.55	−43.170	−36.810
2	0.94 + 0.24 T_a × EVI	LR	0.69	−109.94	−103.59
3	**0.81 + 0.13 EVI × PAR**	**LR**	**0.74**	**−137.74**	**−131.39**
4	−2.08 + 5.28 EVI + 0.07 PAR	MR	0.72	−125.08	−115.55
5	−2.96 + 4.50 EVI + 0.05 PAR + 0.10 T_a	MR	0.76	−149.17	−136.47
6	Artificial Neural Network		–	−181.35	−140.07
Response variable: ELUE					
1	−0.16 + 0.88 EVI	LR	0.85	−1007.91	−1001.55
2	−0.07 + 0.03 T_a × EVI	LR	0.86	−1018.83	−1012.48
3	−0.06 + 0.01 EVI × PAR	LR	0.76	−924.37	−918.02
4	**−0.29 + 0.81 EVI + 0.008 T_a**	**MR**	**0.88**	**−1034.57**	**−1025.04**
5	−0.20 + 0.87 EVI + 0.001 PAR	MR	0.85	−1010.70	−1001.17
6	−0.27 + 0.80 EVI − 0.0008 PAR + 0.001 T_a	MR	0.87	−1034.16	−1021.46
7	Artificial Neural Network		–	−1033.37	−992.080
Response variable: EWUE					
1	**−0.53 + 7.35 EVI**	**LR**	**0.78**	**−177.13**	**−170.78**
2	0.30 + 0.25 T_a × EVI	LR	0.72	−135.27	−128.92
3	0.31 + 0.12 EVI × PAR	LR	0.70	−118.03	−111.67
4	−0.90 + 7.20 EVI + 0.01 PAR	MR	0.78	−178.03	−168.50
5	−0.89 + 7.11 EVI + 0.02 T_a	MR	0.79	−177.19	−167.66
6	−0.98 + 7.13 EVI + 0.01 PAR + 0.01 T_a	MR	0.78	−176.30	−163.59
7	Artificial Neural Network		–	−187.10	−145.81

LR: linear regression, MR: multiple regression, EVI: enhanced vegetation index, PAR: photosynthetically active radiation, T_a: air temperature, R^2: the coefficient of determination, AIC: Akaike's information criterion, and SBC: Schwarz's Bayesian criterion.

($EWUE_{Pred}$) as:

$$ELUE_{Pred} or EWUE_{Pred} = f(EVI, T_a, PAR, T_a \times EVI, PAR \times EVI, T_a + EVI, PAR + EVI) \quad (4)$$

We used the stepwise selection method to select the most significant variable(s). In order to evaluate its potential for providing better estimates of ELUE and EWUE, we also developed predictive relationships for these quantities using the artificial neural network (ANN) technique. The ANN technique employs complex nonlinear transformations and provides the probability of response variables using mathematical functions. Only those variables identify as the most significant in the regression analysis were considered in this exercise. For example, EVI and T_a were used as predictor variables to estimate ELUE, and EVI was used as a predictor variable to estimate EWUE. Finally, we selected the model based on several fit statistics such as the coefficient of determination (R^2), Akaike's information criterion (AIC), and Schwarz's Bayesian criterion (SBC). Regression and ANN analyses were performed in SAS Enterprise Miner 12.3 software (SAS Institute Inc., Cary, NC, USA).

Once the most significant model was developed, $ELUE_{Pred}$ and $EWUE_{Pred}$ were determined for the validation dataset to estimate GPP (GPP_{ELUE}) and ET (ET_{EWUE}) as:

$$GPP_{ELUE} = ELUE_{Pred} \times PAR \quad (5)$$

$$ET_{EWUE} = \frac{GPP_{ELUE}}{EWUE_{Pred}} \quad (6)$$

2.5. Comparison of other GPP and ET models

2.5.1. GPP models

We compared the performance of our parameterized ELUE-based GPP model (GPP_{ELUE}) with the performances of other widely used GPP models that estimate GPP by integrating EVI and climate variables such as temperature or radiation, namely TG, GR, and VI models. We also compared the performance of GPP_{ELUE} with GPPs predicted using a statistical ($GPP_{StatMod}$) and ANN (GPP_{ANN}) models, and the standard GPP_{MOD17} product. The same calibration and validation datasets were used to calibrate and validate all GPP models. The GPP_{MOD17} dataset was also divided into calibration and validation datasets. Here we briefly summarize GPP models used in this study.

2.5.1.1. Temperature and Greenness model. The TG model estimates GPP as (Sims et al., 2008):

$$GPP_{TG} = EVI_{scaled} \times LST_{scaled} \times m \quad (7)$$

where m is a scalar and is determined from the calibration dataset, while EVI_{scaled} and LST_{scaled} are calculated as:

$$EVI_{scaled} = EVI - 0.1 \quad (8)$$

$$LST_{scaled} = \min\left(\frac{LST}{30}, 2.5 - 0.05 \times LST\right) \quad (9)$$

2.5.1.2. Greenness and radiation model. The GR model estimates GPP as (Gitelson et al., 2006):

$$GPP_{GR} = PAR \times EVI \times m \quad (10)$$

where m is a scalar and is determined from the calibration dataset.

2.5.1.3. Vegetation index model. The VI model estimates GPP as (Wu et al., 2010):

$$GPP_{VI} = PAR \times EVI \times EVI \times m \quad (11)$$

where m is a scalar and is determined from the calibration dataset.

2.5.1.4. Statistical and ANN models. The relationship of GPP_{EC} with EVI and major climate variables (T_a and PAR) were analyzed for the calibration dataset to obtain the best predictive GPP estimation ($GPP_{StatMod}$) as:

$$GPP_{EC} = f(EVI, T_a, PAR, T_a \times EVI, PAR \times EVI, T_a + EVI, PAR + EVI) \quad (12)$$

In addition, we also performed ANN using EVI and PAR as predictor variables for estimating GPP (GPP_{ANN}) as mentioned earlier in Section 2.4.

2.5.2. ET models

The relationship of ET_{EC} with EVI and major climate variables (T_a and PAR) were analyzed for the calibration dataset to obtain the best predictive ET estimation ($ET_{StatMod}$) as:

$$ET_{EC} = f(EVI, T_a, PAR, Ta \times EVI, PAR \times EVI, T_a + EVI, PAR + EVI) \quad (13)$$

In addition, we also performed ANN using EVI and PAR as predictor variables for estimating ET (ET_{ANN}). We compared the performance of the parameterized EWUE-based ET model (ET_{EWUE}) with $ET_{StatMod}$, ET_{ANN}, and the standard ET_{MOD16} product. The same calibration and validation datasets were used for ET models as well. The ET_{MOD16} dataset was also divided into calibration and validation datasets.

2.6. Model performance evaluation

The modeled ELUE, EWUE, GPP, and ET values were compared against $ELUE_{EC}$, $EWUE_{EC}$, GPP_{EC}, and ET_{EC}, respectively, to assess the validity of the models. We used several fit statistics such as regression slopes, R^2, and root mean squared error (RMSE) to evaluate the model agreement and bias.

3. Results

3.1. Seasonal and interannual variations in GPP_{EC} and ET_{EC}

The seasonal and interannual variations in GPP_{EC} and ET_{EC} followed the same patterns at all three sites (Fig. 1). Both GPP_{EC} and ET_{EC} started to increase ($GPP_{EC} > 1$ g C m^{-2} d^{-1} and $ET_{EC} > 1$ mm d^{-1}) at the beginning of June, reached a maximum in July, and declined to pre-season value ($GPP_{EC} < 1$ g C m^{-2} d^{-1} and $ET_{EC} < 1$ mm d^{-1}) by late September. Thus, the active growing season for maize spanned from early June to late September. Generally, maize is sown in early to mid-May and harvested in mid- to late October at these sites. Peak GPP_{EC} and ET_{EC} values over the study period at three maize sites are presented in Table 3. Results show that peak GPP values were mostly similar at all sites, but peak ET values were slightly smaller at rainfed (US-Ne3) site than irrigated (US-Ne1 and US-Ne2) sites. In addition, peak ET showed larger interannual variability than did peak GPP at all sites (Fig. 1).

3.2. Seasonal and interannual variations in $ELUE_{EC}$, $EWUE_{EC}$, EVI, and PAR

The seasonal and interannual variations in $ELUE_{EC}$, $EWUE_{EC}$, and EVI followed the same patterns at all sites (Fig. 2). Similar to GPP_{EC} and ET_{EC}, $ELUE_{EC}$, $EWUE_{EC}$, and EVI started to increase at the beginning of June, reached a maximum in July, and declined to pre-season value by late September. As a result, EVI showed strong correlations with $ELUE_{EC}$ (Pearson's correlation coefficient, r = 0.93, 0.93, and 0.87 at US-Ne1, US-Ne2, and US-Ne3, respectively) and $EWUE_{EC}$ (r = 0.88, 0.91, 0.87 at US-Ne1, US-Ne2, and US-Ne3, respectively) at all sites. Peak $ELUE_{EC}$, $EWUE_{EC}$, EVI, and PAR values over the study period at three maize sites are presented in Table 3. The ranges of peak values were 0.40–0.55 g C mol^{-1} PAR for $ELUE_{EC}$, 4.22–5.81 g C mm^{-1} ET for $EWUE_{EC}$, 0.60–0.82 for EVI, and 49–61 mol m^{-2} d^{-1} for PAR across sites.

3.3. Quantitative relationships of GPP_{EC}, ET_{EC}, $ELUE_{EC}$, and $EWUE_{EC}$ with EVI and climate variables

Quantitative relationships of 8-day composite values of GPP_{EC}, ET_{EC}, $ELUE_{EC}$, and $EWUE_{EC}$ were examined with EVI and climate variables across three sites (Table 1). Results show that EVI was strongly correlated with GPP_{EC} (r = 0.87), ET_{EC} (r = 0.74), $ELUE_{EC}$ (r = 0.91), and $EWUE_{EC}$ (r = 0.86). The GPP_{EC}-EVI and ET_{EC}-EVI relationships were further improved by coupling of EVI with T_a or PAR. In addition, GPP_{EC} and ET_{EC} were more strongly correlated with the product of EVI and PAR (EVI × PAR, r = 0.93 and 0.86, respectively) than with the product of EVI and T_a (EVI × T_a, r = 0.91 and 0.83, respectively). As a result, simple and robust statistical models were developed from the calibration dataset to estimate GPP and ET (Table 2) as:

$$GPP_{StatMod} = 0.81(EVI \times PAR) - 5.53, R^2 = 0.88, P < 0.001 \quad (14)$$

$$ET_{StatMod} = 0.13(EVI \times PAR) + 0.81, R^2 = 0.74, P < 0.001 \quad (15)$$

Results show that coupling of EVI with T_a (EVI × T_a) slightly improved the $ELUE_{EC}$-EVI relationship (r = 0.92 vs. 0.91) but not the $EWUE_{EC}$-EVI relationship (r = 0.83 vs. 0.86) compared to EVI alone (Table 1). Similarly, coupling of EVI with PAR (EVI × PAR) did not improve the $ELUE_{EC}$-EVI (r = 0.86 vs. 0.91) and $EWUE_{EC}$-EVI (r = 0.82 vs. 0.86) relationships compared to EVI alone. As a result, simple and robust statistical models were developed from the calibration dataset to estimate ELUE and EWUE (Table 2) as:

$$ELUE_{Pred} = 0.008\,T_a + 0.81EVI - 0.29, R^2 = 0.88, P < 0.001 \quad (16)$$

$$EWUE_{Pred} = 7.35EVI - 0.53, R^2 = 0.78, P < 0.001 \quad (17)$$

Residual plots of the above mentioned four selected regression models and ANN models for predicting GPP, ET, ELUE, and EWUE did not show any systematic pattern (Fig. S1), indicating that the models fit the data well.

3.4. Comparison of predicted ELUE and EWUE with $ELUE_{EC}$ and $EWUE_{EC}$

Predicted ELUE using a multiple regression that uses T_a and EVI ($ELUE_{EVI+Ta}$) and ANN ($ELUE_{ANN}$) models, and predicted EWUE using a simple linear regression that uses only EVI ($EWUE_{EVI}$) and ANN ($EWUE_{ANN}$) models were compared against $ELUE_{EC}$ and $EWUE_{EC}$, respectively, for the model validation dataset (Fig. 3). Predicted ELUE and EWUE values agreed well with $ELUE_{EC}$ and $EWUE_{EC}$, respectively. In addition, results show that regression and ANN models provided similar results for predicting ELUE and EWUE (Fig. 3). Thus, for simplicity, we used $ELUE_{EVI+Ta}$ and $EWUE_{EVI}$ to

Table 3
The range of maximum values (8-day) of tower-based gross primary production (GPP_{EC}, $gC\,m^{-2}\,d^{-1}$), evapotranspiration (ET_{EC}, $mm\,d^{-1}$), ecosystem light use efficiency ($ELUE_{EC}$, $gC\,mol^{-1}$ PAR), ecosystem water use efficiency ($EWUE_{EC}$, $gC\,mm^{-1}$ ET), enhanced vegetation index (EVI), and photosynthetically active radiation (PAR, $mol\,m^{-2}\,d^{-1}$) at three maize sites.

Site	GPP_{EC}	ET_{EC}	$ELUE_{EC}$	$EWUE_{EC}$	EVI	PAR
US-Ne1	22.22–24.97	4.73–7.17	0.44–0.55	4.22–5.25	0.65–0.82	49–60
US-Ne2	24.08–24.95	4.68–6.51	0.44–0.53	4.27–5.81	0.69–0.80	54–61
US-Ne3	20.01–24.40	4.72–5.89	0.40–0.53	4.47–5.60	0.60–0.69	52–60

model GPP (GPP_{ELUE}) and ET (ET_{EWUE}), respectively, as shown in Eqs. (5) and (6).

3.5. Comparison of GPP_{EC} with other estimates of GPP

Predicted GPPs (GPP_{ELUE}, GPP_{ANN}, $GPP_{StatMod}$, GPP_{GR}, GPP_{TG}, and GPP_{VI}) from several models and the standard GPP_{MOD17} product were compared against GPP_{EC} for the model validation data set (Fig. 4). When compared to GPP_{EC}, the parameterized ELUE model demonstrated better performance in predicting GPP than did widely used GPP models (GR, TG, and VI) and the standard GPP_{MOD17} product. The GPP_{ANN} and $GPP_{StatMOD}$ also showed better performance in predicting GPP than did GPP_{GR}, GPP_{TG}, GPP_{VI}, and GPP_{MOD17}.

3.6. Comparison of ET_{EC} with other estimates of ET

Predicted ETs (ET_{EWUE}, ET_{ANN}, $ET_{StatMod}$, and ET_{MOD16}) from several models and the standard ET_{MOD16} product were compared against ET_{EC} for the model validation data set (Fig. 5). When compared to ET_{EC}, the parameterized EWUE model, ANN, and a statistical model showed similar performance in predicting ET. Results show that those ET estimates were substantially improved compared to the standard ET_{MOD16} product.

4. Discussion

Understanding of the seasonal dynamics and interannual variations in GPP, ET, ELUE, and EWUE, and the underlying controlling mechanisms can enhance our ability to predict how climate change may affect carbon and water budgets of maize ecosystems. Results showed that peak GPP_{EC}, $ELUE_{EC}$, and $EWUE_{EC}$ values were mostly similar at all sites. A previous study also reported a similar WUE (or biomass transpiration efficiency = total plant biomass/growing season transpiration) at these irrigated and rainfed sites (Suyker and Verma, 2009). However, peak ET_{EC} of rainfed maize site was smaller than that of irrigated sites. Similarly, peak EVI of rainfed site was also smaller than that of irrigated sites. In addition, peak ET_{EC} showed larger interannual variability than did peak GPP_{EC} (Fig. 1), likely due to differences in soil moisture over years due to variations in rainfall, while differences in GPP_{EC} were not explained by the differences in soil moisture at the irrigated (US-Ne2) and rainfed (US-Ne3) sites (Yuan et al., 2015). For example, peak GPP_{EC} in 2004 at US-Ne1 was similar to other years, but peak ET_{EC} was the lowest in 2004 (Fig. 1) when July and August were dry (72 mm below normal) (Suyker and Verma, 2008).

As in several previous studies (Dong et al., 2015; Ma et al., 2014; Nagler et al., 2005; Sims et al., 2008; Wagle et al., 2015b, 2014), we observed strong correlations of EVI with GPP_{EC} and ET_{EC} (Table 1). In addition, EVI showed strong correlations with $ELUE_{EC}$ and $EWUE_{EC}$ (Table 1), indicating that EVI could be used as a measure of $ELUE_{EC}$ and $EWUE_{EC}$ in maize. Our results show that the relationships of EVI with GPP_{EC} and ET_{EC} were further improved by coupling EVI with PAR compared to EVI alone. As a result, simple statistical and ANN models developed by integrating EVI and PAR demonstrated better performance in predicting GPP compared to estimates from most widely used GPP models (GR, TG, and VI) and the standard GPP_{MOD17} product (Fig. 4). Similarly, simple statistical and ANN models developed by integrating EVI and PAR provided significantly improved estimates of ET compared to the standard ET_{MOD16} product (Fig. 5).

Our results demonstrate that ELUE and EWUE of maize can be predicted at 8-day intervals with reasonable accuracy using the MODIS-derived EVI and climate variables (Fig. 3). Previous studies also correlated LUE with vegetation indices, including normalized difference vegetation index (NDVI) and EVI in crop (Wu et al., 2009) and peatland ecosystems (Schubert et al., 2010), showing the potential of vegetation indices to estimate LUE. Typical methods of LUE simulation require prior specification of a biome-scale maximum LUE and additional climate input to modulate the maximum LUE for the growing season (Running et al., 2004). The dependency on climate input and biome-scale maximum LUE can induce significant uncertainties in estimates of GPP and limit its global application (Heinsch et al., 2006; Zhao et al., 2006). Further, most LUE-based models account only for the impacts of temperature and water or vapor pressure deficit on LUE (Running et al., 2004; Xiao et al., 2004). Although previous studies have shown the potential of PRI in tracking LUE at the leaf level based on ground spectral measurements (Filella et al., 2009; Gamon et al., 1997) and satellite observations (Drolet et al., 2008; Hall et al., 2008; Hilker et al., 2009), high sensitivity of PRI to numerous extraneous effects such as canopy structure and the view observer geometry prevents its application at large spatial (landscape-to-global) scales, thereby requiring upscaling algorithms to account for structural differences in vegetation (Hilker et al., 2010).

The assumption of a constant maximum value of ELUE or EWUE for the entire growing season, across years, and across sites for a biome type is very common in GPP and ET models (Alfieri et al., 2009; Running et al., 2004; Wagle et al., 2014; Zhang et al., 2009). Our results illustrated that there was a clear seasonality of ELUE and EWUE, and the maximum values of ELUE and EWUE varied year-to-year at the same site (Fig. 2), indicating that ELUE and EWUE are not constant properties. Because of the assumption of a constant LUE for the entire growing season, our results show that GR and TG models overestimated GPP in the lower range of GPP (i.e., $GPP < 10\,g\,C\,m^{-2}\,d^{-1}$ during the early and late growing season, Fig. 4). Our results suggest that accurate estimations of GPP and ET require an improved representation of seasonal dynamics and interannual variations in ELUE and EWUE. The ELUE and EWUE parameterization approaches using EVI and climate variables can avoid an important source of uncertainty in GPP and ET that arises from spatial and temporal variations in ELUE and EWUE, respectively. Another important advantage of this approach is that it does not require prior information of species composition and their contributions on the measured values of CO_2 fluxes and ET, especially in mixed vegetation ecosystems (e.g., mixed C_4 and C_3 species). Typical methods of GPP and ET simulations use different maximum ELUE and EWUE values for C_4 and C_3 species.

Despite a close correspondence of predicted values of GPP, ET, ELUE, and EWUE with GPP_{EC}, ET_{EC}, $ELUE_{EC}$, and $EWUE_{EC}$, there were some large discrepancies. These discrepancies can be attributed to multiple sources of errors or uncertainties. Some errors or uncer-

tainties might come from errors and uncertainties in GPP_{EC} and ET_{EC} measurements as energy balance closure errors can be 10–30% (Twine et al., 2000). Substantial uncertainties in GPP data can arise from partitioning of NEE to GPP and ecosystem respiration (Hagen et al., 2006) and gap fillings of EC data (Richardson and Hollinger, 2007). In addition, some errors or uncertainties in ET data can arise from not filtering ET data for irrigation or rainfall events although 8-day composite values were used. The simplified assumption that was made in estimating ELUE using EVI and T_a, and in estimating EWUE using only EVI also introduced some uncertainties as EVI × T_a explained 85% and EVI explained 74% of the variations in $ELUE_{EC}$ and $EWUE_{EC}$, respectively, for our dataset (Table 1). The sensitivity of $ELUE_{EC}$ and $EWUE_{EC}$ to input parameters (EVI and T_a) can also introduce some uncertainties in estimations of ELUE and EWUE, and ultimately in estimations of GPP and ET. To further investigate the sensitivity of $ELUE_{EC}$ and $EWUE_{EC}$ to input parameters, we examined ELUE residuals ($ELUE_{Pred} - ELUE_{EC}$) against EVI and T_a, and EWUE residuals ($EWUE_{Pred} - EWUE_{EC}$) against EVI. Lack of any discernible trends of residuals against EVI or T_a indicated that there were no systematic errors associated with input parameters (Fig. S2). However, large scatter of residuals still exist which can affect the agreement between the modeled and observed GPP and ET. Note that the modeled and observed values cannot match exactly even if all the modeling or observed errors or uncertainties could be removed (Taylor, 2001). However, we found that the parameterized ELUE model demonstrated better performance in predicting GPP compared to most widely used GPP models (GR, TG, and VI) and the standard GPP_{MOD17} product (Fig. 4). Similarly, ET estimates from the parameterized EWUE model, statistical, and ANN models were substantially improved compared to the standard ET_{MOD16} product (Fig. 5). These results demonstrate that the parameterized ELUE and EWUE using EVI and climate variables can be used for predicting maize GPP and ET with reasonable accuracy without dependence on look-up table or coarse resolution climate data to estimate ELUE and EWUE.

5. Conclusions

Seasonally, EVI tracked closely with GPP_{EC}, ET_{EC}, $ELUE_{EC}$, and $EWUE_{EC}$, indicating that it is the primary factor controlling the seasonal variations in maize GPP_{EC}, ET_{EC}, $ELUE_{EC}$, and $EWUE_{EC}$. The relationship between EVI and $ELUE_{EC}$ was further improved by coupling EVI with T_a compared to EVI alone. Coupling of EVI with T_a or PAR did not improve the relationship between EVI and $EWUE_{EC}$ compared to EVI alone. Based on these results, we developed novel models to estimate ELUE and EWUE at 8-day intervals. Our results illustrate that the parameterized ELUE and EWUE models offer new methods of predicting GPP and ET, respectively, with reasonable accuracy. The usefulness of these new approaches should be validated for larger spatial and smaller temporal scales and different land cover types in the future. These analyses will be helpful for the development of future GPP and ET estimation models, and improving our understanding of the responses of terrestrial ecosystems to future climate change.

Acknowledgements

This study was supported in part by a research grant (Project No. 2013-69002) through the USDA National Institute for Food and Agriculture (NIFA)'s Agriculture and Food Research Initiative (AFRI), Regional Approaches for Adaptation to and Mitigation of Climate Variability and Change, and a research grant (IIA-1301789) from the National Science Foundation EPSCoR. Flux and climate data were obtained from the AmeriFlux database (http://ameriflux.lbl.gov/). We would like to thank Dr. Andrew Suyker (University of Nebraska) for the Mead flux tower data.

Appendix: Definition of abbreviations.

GPP_{EC}	Tower-based gross primary production
ET_{EC}	Tower-based evapotranspiration
$ELUE_{EC}$	Tower-based ecosystem light use efficiency
$EWUE_{EC}$	Tower-based ecosystem water use efficiency
$ELUE_{Pred}$	Predicted ELUE using regression model
$EWUE_{Pred}$	Predicted EWUE using regression model
$ELUE_{ANN}$	Predicted ELUE using artificial neural network
$EWUE_{ANN}$	Predicted EWUE using artificial neural network
$ELUE_{EVI+Ta}$	Predicted ELUE using EVI and air temperature
$EWUE_{EVI}$	Predicted EWUE using EVI
GPP_{ELUE}	Predicted GPP using parameterized ELUE model
ET_{EWUE}	Predicted ET using parameterized EWUE model
GPP_{MOD17}	MODIS GPP global product
ET_{MOD16}	MODIS ET global product
GPP_{ANN}	Predicted GPP using artificial neural network
ET_{ANN}	Predicted ET using artificial neural network
GPP_{TG}	Predicted GPP using temperature and Greenness model
GPP_{GR}	Predicted GPP using Greenness and radiation model
GPP_{VI}	Predicted GPP using vegetation index model
$GPP_{StatMod}$	Predicted GPP using statistical model
$ET_{StatMod}$	Predicted ET using statistical model

Appendix A. Supplementary data

Supplementary data associated with this article can be found, in the online version, at http://dx.doi.org/10.1016/j.agrformet.2016.03.009.

References

Alfieri, J.G., et al., 2009. Satellite-based modeling of transpiration from the grasslands in the Southern Great Plains, USA. Global Planet. Change 67 (1), 78–86.
Allen, R.G., Tasumi, M., Trezza, R., 2007. Satellite-based energy balance for mapping evapotranspiration with internalized calibration (METRIC)—model. J. Irrig. Drain. Eng. 133 (4), 380–394.
Baldocchi, D., et al., 2001. FLUXNET: a new tool to study the temporal and spatial variability of ecosystem-scale carbon dioxide, water vapor, and energy flux densities. Bull. Am. Meteorol. Soc. 82 (11), 2415–2434.
Bastiaanssen, W., Menenti, M., Feddes, R., Holtslag, A., 1998. A remote sensing surface energy balance algorithm for land (SEBAL). 1. Formulation. J. Hydrol. 212, 198–212.
Bonan, G.B., 1993. Importance of leaf area index and forest type when estimating photosynthesis in boreal forests. Remote Sens. Environ. 43 (3), 303–314.
Choudhury, B.J., Ahmed, N.U., Idso, S.B., Reginato, R.J., Daughtry, C.S., 1994. Relations between evaporation coefficients and vegetation indices studied by model simulations. Remote Sens. Environ. 50 (1), 1–17.
Dong, J., et al., 2015. Comparison of four EVI-based models for estimating gross primary production of maize and soybean croplands and tallgrass prairie under severe drought. Remote Sens. Environ. 162, 154–168.
Drolet, G., et al., 2008. Regional mapping of gross light-use efficiency using MODIS spectral indices. Remote Sens. Environ. 112 (6), 3064–3078.
Emmerich, W.E., 2007. Ecosystem water use efficiency in a semiarid shrubland and grassland community. Rangel. Ecol. Manag. 60 (5), 464–470.
Filella, I., et al., 2009. PRI assessment of long-term changes in carotenoids/chlorophyll ratio and short-term changes in de-epoxidation state of the xanthophyll cycle. Int. J. Remote Sens. 30 (17), 4443–4455.
Gamon, J., Penuelas, J., Field, C., 1992. A narrow-waveband spectral index that tracks diurnal changes in photosynthetic efficiency. Remote Sens. Environ. 41 (1), 35–44.
Gamon, J., Serrano, L., Surfus, J., 1997. The photochemical reflectance index: an optical indicator of photosynthetic radiation use efficiency across species, functional types, and nutrient levels. Oecologia 112 (4), 492–501.
Gillies, R., Kustas, W., Humes, K., 1997. A verification of the 'triangle' method for obtaining surface soil water content and energy fluxes from remote measurements of the Normalized Difference Vegetation Index (NDVI) and surface. Int. J. Remote Sens. 18 (15), 3145–3166.
Gitelson, A.A., et al., 2006. Relationship between gross primary production and chlorophyll content in crops: implications for the synoptic monitoring of vegetation productivity. J. Geophys. Res.: Atmos. 111 (D8), D08S11.
Glenn, E.P., Huete, A.R., Nagler, P.L., Hirschboeck, K.K., Brown, P., 2007. Integrating remote sensing and ground methods to estimate evapotranspiration. Crit. Rev. Plant Sci. 26 (3), 139–168.
Glenn, E.P., Huete, A.R., Nagler, P.L., Nelson, S.G., 2008. Relationship between remotely-sensed vegetation indices, canopy attributes and plant physiological

processes: what vegetation indices can and cannot tell us about the landscape. Sensors 8 (4), 2136–2160.
Guanter, L., et al., 2014. Global and time-resolved monitoring of crop photosynthesis with chlorophyll fluorescence. Proc. Natl. Acad. Sci. U. S. A. 111 (14), E1327–E1333.
Hagen, S., et al., 2006. Statistical uncertainty of eddy flux-based estimates of gross ecosystem carbon exchange at Howland Forest, Maine. J. Geophys. Res.: Atmos. 111 (D8), 1984–2012.
Hall, F.G., et al., 2008. Multi-angle remote sensing of forest light use efficiency by observing PRI variation with canopy shadow fraction. Remote Sens. Environ. 112 (7), 3201–3211.
Heinsch, F.A., et al., 2006. Evaluation of remote sensing based terrestrial productivity from MODIS using regional tower eddy flux network observations geoscience and remote sensing. IEEE Trans. 44 (7), 1908–1925.
Hilker, T., et al., 2009. An assessment of photosynthetic light use efficiency from space: modeling the atmospheric and directional impacts on PRI reflectance. Remote Sens. Environ. 113 (11), 2463–2475.
Hilker, T., et al., 2010. Remote sensing of photosynthetic light-use efficiency across two forested biomes: spatial scaling. Remote Sens. Environ. 114 (12), 2863–2874.
Jenkins, J., et al., 2007. Refining light-use efficiency calculations for a deciduous forest canopy using simultaneous tower-based carbon flux and radiometric measurements. Agric. Forest Meteorol. 143 (1), 64–79.
Jin, C., et al., 2013. Phenology and gross primary production of two dominant savanna woodland ecosystems in Southern Africa. Remote Sens. Environ. 135 (0), 189–201.
Kalma, J.D., McVicar, T.R., McCabe, M.F., 2008. Estimating land surface evaporation: a review of methods using remotely sensed surface temperature data. Surv. Geophys. 29 (4–5), 421–469.
Kustas, W., Norman, J., 1996. Use of remote sensing for evapotranspiration monitoring over land surfaces. Hydrol. Sci. J. 41 (4), 495–516.
Law, B., et al., 2002. Environmental controls over carbon dioxide and water vapor exchange of terrestrial vegetation. Agric. Forest Meteorol. 113 (1), 97–120.
Liou, Y.-A., Kar, S.K., 2014. Evapotranspiration estimation with remote sensing and various surface energy balance algorithms—a review. Energies 7 (5), 2821–2849.
Ma, X., et al., 2014. Parameterization of an ecosystem light-use-efficiency model for predicting savanna GPP using MODIS EVI. Remote Sens. Environ. 154, 253–271.
Monteith, J., 1972. Solar radiation and productivity in tropical ecosystems. J. Appl. Ecol. 9 (3), 747–766.
Moreno, A., et al., 2012. Assessment of MODIS imagery to track light-use efficiency in a water-limited Mediterranean pine forest. Remote Sens. Environ. 123, 359–367.
Mu, Q., Heinsch, F.A., Zhao, M., Running, S.W., 2007. Development of a global evapotranspiration algorithm based on MODIS and global meteorology data. Remote Sens. Environ. 111 (4), 519–536.
Nagler, P.L., et al., 2005. Predicting riparian evapotranspiration from MODIS vegetation indices and meteorological data. Remote Sens. Environ. 94 (1), 17–30.
Parazoo, N.C., et al., 2014. Terrestrial gross primary production inferred from satellite fluorescence and vegetation models. Global Change Biol. 20 (10), 3103–3121.
Potter, C.S., et al., 1993. Terrestrial ecosystem production: a process model based on global satellite and surface data. Global Biogeochem. Cycles 7 (4), 811–841.
Prince, S.D., Goward, S.N., 1995. Global primary production: a remote sensing approach. J. Biogeogr., 815–835.
Richardson, A.D., Hollinger, D.Y., 2007. A method to estimate the additional uncertainty in gap-filled NEE resulting from long gaps in the CO_2 flux record. Agric. Forest Meteorol. 147 (3), 199–208.
Roerink, G., Su, Z., Menenti, M., 2000. S-SEBI: a simple remote sensing algorithm to estimate the surface energy balance physics and chemistry of the Earth, Part B: hydrology. Oceans Atmos. 25 (2), 147–157.
Ruimy, A., Jarvis, P., Baldocchi, D., Saugier, B., 1995. CO_2 fluxes over plant canopies and solar radiation: a review. Adv. Ecol. Res. 26, 1–68.
Running, S.W., et al., 2004. A continuous satellite-derived measure of global terrestrial primary production. Bioscience 54 (6), 547–560.
Schubert, P., Lund, M., Ström, L., Eklundh, L., 2010. Impact of nutrients on peatland GPP estimations using MODIS time series data. Remote Sens. Environ. 114 (10), 2137–2145.
Senay, G.B., et al., 2013. Operational evapotranspiration mapping using remote sensing and weather datasets: a new parameterization for the SSEB approach. JAWRA J. Am. Water Resour. Assoc. 49 (3), 577–591.
Sims, D.A., et al., 2008. A new model of gross primary productivity for North American ecosystems based solely on the enhanced vegetation index and land surface temperature from MODIS. Remote Sens. Environ. 112 (4), 1633–1646.
Su, Z., 2002. The surface energy balance system (SEBS) for estimation of turbulent heat fluxes. Hydrol. Earth Syst. Sci. Discuss. 6 (1), 85–100.
Suyker, A.E., Verma, S.B., 2008. Interannual water vapor and energy exchange in an irrigated maize-based agroecosystem. Agric. Forest Meteorol. 148 (3), 417–427.
Suyker, A.E., Verma, S.B., 2009. Evapotranspiration of irrigated and rainfed maize–soybean cropping systems. Agric. Forest Meteorol. 149 (3), 443–452.
Suyker, A.E., Verma, S.B., 2012. Gross primary production and ecosystem respiration of irrigated and rainfed maize–soybean cropping systems over 8 years. Agric. Forest Meteorol. 165, 12–24.
Tan, K.P., Kanniah, K.D., Cracknell, A.P., 2013. The potential of MODIS derived photochemical reflectance index for studying gross primary productivity of oil palm trees, geoscience and remote sensing symposium (IGARSS). 2013 IEEE International. IEEE, 2141–2144.
Tang, X., et al., 2015. Tracking ecosystem water use efficiency of cropland by exclusive use of MODIS EVI data. Remote Sens. 7 (9), 11016–11035.
Taylor, K.E., 2001. Summarizing multiple aspects of model performance in a single diagram. J. Geophys. Res. Atmos. 106 (D7), 7183–7192 (1984–2012).
Turner, D.P., et al., 2003. A cross-biome comparison of daily light use efficiency for gross primary production. Global Change Biol. 9 (3), 383–395.
Twine, T.E., et al., 2000. Correcting eddy-covariance flux underestimates over a grassland. Agric. Forest Meteorol. 103 (3), 279–300.
Verma, S.B., et al., 2005. Annual carbon dioxide exchange in irrigated and rainfed maize-based agroecosystems. Agric. Forest Meteorol. 131 (1), 77–96.
Wagle, P., et al., 2014. Sensitivity of vegetation indices and gross primary production of tallgrass prairie to severe drought. Remote Sens. Environ. 152 (0), 1–14.
Wagle, P., et al., 2015a. Biophysical controls on carbon and water vapor fluxes across a grassland climatic gradient in the United States. Agric. Forest Meteorol. 214–215, 293–305.
Wagle, P., Xiao, X., Suyker, A.E., 2015b. Estimation and analysis of gross primary production of soybean under various management practices and drought conditions. ISPRS J. Photogramm. Remote Sens. 99 (0), 70–83.
Wagle, P., Zhang, Y., Jin, C., Xiao, X., 2015c. Comparison of solar-induced chlorophyll fluorescence, light-use efficiency, and process-based GPP models in maize. Ecol. Appl., http://dx.doi.org/10.1002/15-1434.
Wu, C., et al., 2009. Remote estimation of gross primary production in wheat using chlorophyll-related vegetation indices. Agric. Forest Meteorol. 149 (6), 1015–1021.
Wu, C., Niu, Z., Gao, S., 2010. Gross primary production estimation from MODIS data with vegetation index and photosynthetically active radiation in maize. J. Geophys. Res.: Atmos. 115 (D12), 1984–2012.
Wu, C., et al., 2012. Remote sensing of canopy light use efficiency in temperate and boreal forests of North America using MODIS imagery. Remote Sens. Environ. 118, 60–72.
Xiao, X., et al., 2004. Satellite-based modeling of gross primary production in an evergreen needleleaf forest. Remote Sens. Environ. 89 (4), 519–534.
Yuan, W., et al., 2007. Deriving a light use efficiency model from eddy covariance flux data for predicting daily gross primary production across biomes. Agric. Forest Meteorol. 143 (3), 189–207.
Yuan, W., et al., 2015. Uncertainty in simulating gross primary production of cropland ecosystem from satellite-based models. Agric. Forest Meteorol. 207, 48–57.
Zhang, J., et al., 2009. Satellite-based estimation of evapotranspiration of an old-growth temperate mixed forest. Agric. Forest Meteorol. 149 (6), 976–984.
Zhao, M., Running, S.W., Nemani, R.R., 2006. Sensitivity of moderate resolution imaging spectroradiometer (MODIS) terrestrial primary production to the accuracy of meteorological reanalyses. J. Geophys. Res.: Biogeosci. 111 (G1), 2005–2012.